Definitive screening design applied to cationic & anionic adsorption dyes on Almond shells activated carbon: Isotherm, kinetic and thermodynamic studies

Article *in* Materials Today: Proceedings · August 2022

DOI: 10.1016/j.matpr.2022.07.358

CITATIONS
12

READS
106

6 authors, including:

Hamza Boulika
Faculté des Sciences et Techniques Fès
6 PUBLICATIONS **24** CITATIONS
SEE PROFILE

Maryam Elhajam
Faculty of Sciences and Techniques
16 PUBLICATIONS **127** CITATIONS
SEE PROFILE

Meryem Hajji Nabih
Faculté des Sciences et Techniques Fès
7 PUBLICATIONS **25** CITATIONS
SEE PROFILE

Issam Riffi Karim
Faculté des Sciences et Techniques Fès
1 PUBLICATION **12** CITATIONS
SEE PROFILE

Materials Today: Proceedings xxx (xxxx) xxx

Contents lists available at ScienceDirect

Materials Today: Proceedings

journal homepage: www.elsevier.com/locate/matpr

Definitive screening design applied to cationic & anionic adsorption dyes on Almond shells activated carbon: Isotherm, kinetic and thermodynamic studies

H. Boulika [a,*], M. El Hajam [a,b], M. Hajji Nabih [a], I. Riffi Karim [a,b], N. Idrissi Kandri [a], A. Zerouale [b]

[a] Signals, Systems and Components Laboratory (SSC), Faculty of Sciences and Techniques, Sidi Mohamed Ben Abdellah University, Route Imouzzer, BP2202, Atlas, FEZ, Morocco
[b] Processes, Materials and Environment Laboratory (PME), Faculty of Sciences and Techniques, Sidi Mohamed Ben Abdellah University, Route Imouzzer, BP2202, Atlas, FEZ, Morocco

ARTICLE INFO

Article history:
Available online xxxx

Keywords:
Adsorption
Definitive screening design
Activated Carbon
Almond Shells
Removal dyes
Screening
Optimization

ABSTRACT

The potential use of activated carbon from Almond shells for the removal of Malachite Green (MG) and Methyl Red (MR) respectively. The different factors influencing the adsorption process were screened and optimized in batch using the D.S.D methodology. Isothermal and Kinetic adsorption modeling fits more the Langmuir model and followed pseudo-second-order for both dyes. The positive ΔS° and negative ΔH° values indicate a spontaneous and exothermic adsorption process. The maximum removal of MG was 93.81 % and that of MR was 82.81 %. The characterization of activated carbon after adsorption indicates that this material remains stable and effective.

Selection and peer-review under responsibility of the scientific committee of the Fifth edition of the International Conference on Materials & Environmental Science.

1. Introduction

Synthetic organic dyes are becoming more and more prominent in the majority of industries around the world. Their excess uses are usually dumped into nature, inducing environmental as well as health problems [1,2]. Malachite Green (MG) and Methyl Red (MR), cationic and anionic dyes respectively, are examples of these synthetic dyes. They have been widely used for dyeing leather, silk, wool, and distilleries [3], however, their oral consumption is carcinogenic [4]. The available toxicological information reveals the presence of dyes traces in the tissues of fish and mice Thus, the detection of MG in fishes, animal milk, and other foodstuff designed for human consumption is of great alarm for human health. MR may irritate the skin, eye, and digestive tract [5,6] Removing those dyes from wastewater or treating it in a way to minimize its effects on the environment is essential.

To resolve these problems, several solutions for water treatment have been proposed such as membrane techniques [7], chemical oxidation [8,9], coagulation-flocculation [10], and anaerobic degradation using various microorganisms [11]. Some of these techniques are proving effective, but are limited to excessive chemical use and coating build-up [12]. The activated carbon adsorption technique is found to be among the best dye removal techniques in terms of initial cost, simplicity of use, and non-toxicity of the used adsorbents [13,14].

Activated carbon (AC) prepared from lignocellulosic waste is found to be more efficient and less expensive compared to the commercial one [15]. Activated carbon based Almond Shell has been reported previously by Demirbas et al. to be an effective adsorbent of Cr(VI) [16]. Mohan et al. used Almond shells to develop a magnetic AC to remove trinitrophenol from an aqueous solution [17]. Similarly, Hashemian et al. prepared AC based on Almond shells by a physical method for the adsorption of 2-picoline in an aqueous solution [18]. Actually, there is a lack of works that study the influence of factors on the adsorption process using new approaches, and it is interesting to study the efficiency of our activated carbon prepared from Almond shells as a low-cost adsorbent of dissolved dyes in waters.

The variables affecting the adsorption process were optimized by a new experimental design, called the Definitive Screening Design (DSD). The application of this design ensures the low-cost preservation of the method by using the least number of experiments, the obtained data can be processed with a high degree of inevitability [19].

The objective of this work is to see the effectiveness of Almond shell activated carbon as a low-cost adsorbent into cationic and

* Corresponding author.
E-mail address: Hamza.boulika@usmba.ac.ma (H. Boulika).

https://doi.org/10.1016/j.matpr.2022.07.358
2214-7853/
Selection and peer-review under responsibility of the scientific committee of the Fifth edition of the International Conference on Materials & Environmental Science.

anionic dyes namely, MG and MR, by screening and optimizing the factors influencing the adsorption process in order to obtain a maximum removal rate. Physicochemical characterization of activated carbon after adsorption by Fourier Transform Infrared Spectrophotometry (FT-IR), Scanning Electron Microscopy (SEM), and X-ray diffraction was carried out to ensure its efficiency. Kinetic, thermodynamic, and isothermal equilibrium studies were performed to know the nature of the adsorption process.

2. Material and methods

2.1. Material

The activated carbon used was previously prepared from Almond shells. They were chemically activated by phosphoric acid and then pyrolyzed in a vacuum carbonization system developed in the laboratory. Table 1 summarizes the physicochemical characteristics of the prepared activated carbon.

During this study, we used Malachite Green (MG) ($\mathbf{C_{23}H_{25}N_2Cl}$) as a cationic dye and Methyl Red (MR) ($\mathbf{C_{15}H_{15}N_3O_2}$) as an anionic type. The stock solutions were prepared at a concentration of 500 mg/l. The solutions used for all the tests were prepared by diluting the stock solutions appropriately.

3. Methods

3.1. Definitive screening design

In order to quantify and elucidate the effects of the influencing factors, namely: initial dye concentrations, contact time, temperature, pH of the solutions, and the amount of adsorbent on the removal rate of MG and MR, Definitive screening design DSD [20] is used to estimate the linearity of the effects. A new three-level multivariate analysis (MVA) approach is used to select the significant variables. The evaluation of the active effects, two-factor interaction effects, and purely quadratic effects is done in one step [21]. The multiple regression equation (Eq. (1)) was developed to predict the response in order to analyze the effect of each parameter influencing the adsorption and the effects of its interactions with the other parameters. The significance of each coefficient is tested based on the H_0 hypothesis which assumes that a given coefficient is not significant. The evaluation of the significance of an effect is based on its "p-value", i.e., the probability of rejecting the H_0 hypothesis. The effect is considered significant when p is<0.05. The number of experiments N for DSD is only 2 k + 1 or 2 k + 3, for a pair or impair number of factors k, respectively [22,23]. The measured response in this study is the adsorption rate. The specific levels for each factor are shown in Table 2. A total of 20 experiments were designed; 13 experiments were performed, 4 additional experiments, and 2 additional central experiments for a better estimation of "lack of fit". By invoking the principle of effect sparsity, one strategy can determine the truly active effects [24].

$$Y = a_0 + a_1.X_1 + \cdots + a_n.X_n + \sum_{i=1}^{n} a_{ij}.X_iX_j + \sum_{i-1}^{n} a_{ii}.X_i^2 \quad (1)$$

Where Y represents the measured response, a_0 is the model constant, a_i is the regression coefficients, X_i is the independent variable, X_i, X_j are the interaction terms and X_i^2 is the quadratic term. Data analysis was performed using the Box-Cox transformation [25].

Table 1
Physicochemical characteristics of activated carbon.

Characteristics	Value
Humidity (%)	10.53 ± 03.66
Ash contents (wt%)	14.95 ± 1.43
pH_{pzc}	4.5
Iodine index (mg/g)	824.85
Oxygen functions (meq/g)	
Strong carboxylic acid	0.94
Lactone and weak carboxylic acid	0.089
Hydroxyl and phenol	0.67
Total acid functions	1.699
Basic functions	0.52

3.1.1. Adsorption study

The adsorption study was carried out in batch, using a volume of 20 ml of dye solution at a defined concentration in the presence of a known quantity of adsorbent. Each mixture was stirred and kept at a given temperature in a thermostated water bath for a certain time. The initial pH of the solutions was adjusted with a solution of NaOH and HCl (0.1 M). The mixtures were then centrifuged by a hercuvan TT-14500 PRO microcentrifuge. The residual dye concentration was quantified using a Biobase BK-D580 UV–Visible spectrophotometer.

The adsorption capacity q_e (mg/g) and percent removal (%R) of the dye were calculated using equations (2) and (3):

$$q_e = \frac{C_0 - C_e}{m} \times V \quad (2)$$

$$\%R = \frac{C_0 - C_e}{C_0} \times 100 \quad (3)$$

With, C_o and C_e the initial and equilibrium dye concentrations (mg/l) respectively, V the volume (l), and m the mass of the adsorbent (g).

3.1.2. Kinetic models of adsorption

The kinetics of the adsorption was studied using three models, namely: pseudo-first-order [26] pseudo-second order [27], and Elovich [28]. The conformity of the experimental data with the predicted values by the applied models was expressed by the fitted correlation coefficients (R^2_{ajd}) and the probability value.

- The pseudo-first order model is expressed by Eq (4):

$$log(q_e - q_t) = loglog(q_e) - \frac{K_f}{2.303} \times t \quad (4)$$

With, k_f the pseudo-first order kinetic constant (min^{-1}), q_t and q_e the adsorption capacities at time t and at equilibrium respectively ($mg.g^{-1}$) and t the contact time (min).

- The pseudo-second order model is expressed by Eq. (5)

$$\frac{t}{q_t} = \frac{1}{K_s \times q_e^2} + \frac{t}{q_e} \quad (5)$$

With, k_s the pseudo-first order kinetic constant ($g.mg^{-1}.min^{-1}$) q_t and q_e the adsorption capacities at time t and equilibrium respectively ($mg.g^{-1}$) and t the contact time (min).

- The Elovich equation (6) allows deducing in general the chemisorption process and covers a wide range of slow adsorption. It is often valid for systems with heterogeneous adsorption surfaces.

$$q_t = \frac{1}{\beta} \times (\alpha \times \beta) + \frac{1}{\beta} ln(t) \quad (6)$$

With, α the initial adsorption rate ($mg.g^{-1}.min^{-1}$), β the desorption constant ($g.mg^{-1}$) for one experiment, q_t the adsorption capacity at an instant t ($mg.g^{-1}$) and t the contact time (min).

Table 2
Factors studied and their levels.

Dye	Factor	Coded factor	Level		
			−1	0	+1
	Time (min)	X1	1	10.5	20
	Temperature (°C)	X2	15	25	35
	Adsorbent quantity (g)	X3	0.01	0.055	0.1
MG	pH	X4	2	5	8
	Dye concentration (ppm)	X5	10	105	200
MR	pH	X4	2	4	6
	Dye concentration (ppm)	X5	10	55	100

3.1.3. Modeling of adsorption isotherms

The adsorption isotherm is used to describe the equilibrium distribution of the dye between the solid and liquid phase at a given temperature when equilibrium is reached. Langmuir and Freundlich's isotherms have been applied to fit the equilibrium data [29]. Each isotherm is expressed by relative constants that characterize the surface properties and indicate the adsorption capacity of the material [30].

3.1.3.1. Langmuir isotherm. Langmuir's model assumes that adsorption is monolayer and occurs on the surface of the solid with identical homogeneous sites [31]. It also suggests that no further adsorption takes place once the active sites are covered with dye molecules. The saturated Langmuir isotherm is represented by equation (7):

$$\frac{C_e}{q_e} = \frac{1}{q_m \times K_L} + \frac{C_e}{q_t} \tag{7}$$

With, C_e the equilibrium concentration (mg. l^{-1}), q_t and q_e the adsorption capacities at time t and equilibrium respectively (mg. g^{-1}), q_m is the theoretical maximum adsorption capacity (mg.g^{-1}) and K_L a constant denoting the adsorption energy and the affinity of the binding sites (l/mg).

3.1.3.2. Freundlich isotherm. The Freundlich isotherm is an empirical model assuming that the thermal distribution on the surface of the adsorbent is non-uniform, corresponds to a heterogeneous adsorption [32]. It is expressed by the equation (8):

$$log(q_e) = log(K_f) + \frac{1}{n_f} \times log(C_e) \tag{8}$$

With, n_f and K_f (mg/g) the two Freundlich constants giving an indication of the adsorption intensity and capacity, respectively. The degree of non-linearity between the solution concentration and the adsorbent depends on the value of n_f:

- If $\boldsymbol{n_f}$ = 1, the adsorption is linear;
- If $\boldsymbol{n_f}$ < 1, the adsorption process is chemical;
- if $\boldsymbol{n_f}$ greater than 1, the adsorption process is physical.

3.1.4. Thermodynamic study

The thermodynamic adsorption behaviors of MG and MR on AC were studied using thermodynamic functions such as, Gibbs free energy change (ΔG°), enthalpy (ΔH°) and entropy (ΔS°) using equations (9) and (10):

$$\Delta G^{\circ} = -R.T.Ln(K_0) \tag{9}$$

Table 3
Pareto chart analysis.

Dye	Source	logWorth	P-value
MG	pH*pH	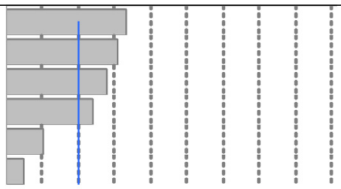	0.00045
	Adsorbent quantity		0.00082
	Adsorbat concentration		0.00158
	pH		0.00388
	pH*Adsorbent quantity		0.08847
	pH*Adsorbat concentration		0.30514
MR	Adsorbent quantity		0.00000
	pH		0.00000
	pH*Adsorbent quantity		0.00014
	Adsorbent quantity *Adsorbent quantity		0.00108
	pH*pH		0.13397

Table 4
Lack of fit results.

Dye	Source	DDL	Sum square	Mean square	F ratio	Prob. > F
MG	Lack of Fit	3	130.40	43.47	2.0966	0.16
	Pure error	11	228.05	20.73		
	Total error	14	358.45			
MR	Lack of Fit	5	172.23980	34.4480	5.1455	0.06
	Pure error	5	33.47363	6.6947		
	Total error	10	205.71343			

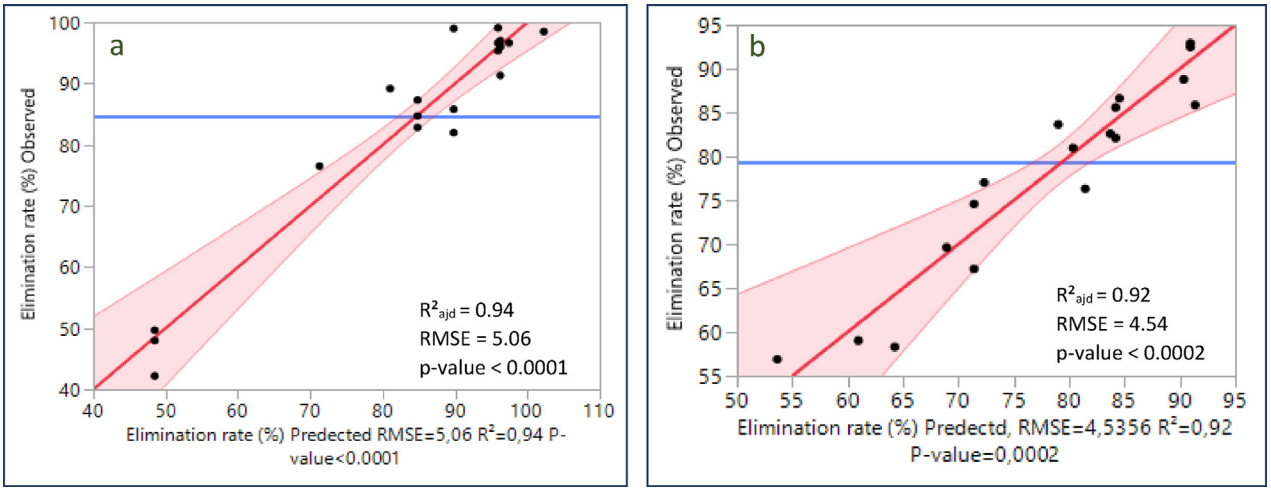

Fig. 1. Scatterplots of experimental and predicted values modeled by DSD for MG (a) and MR (b).

Table 5
Significant coefficients of the principal parameters, quadratic coefficients, and two-factor interactions for the obtained model of MG and MR adsorption.

Dye	Parameter	Estimated parameters	Standard error	t ratio	Prob. > |t|
MG	Constant	90.948	2.1564	42.18	<0.0001
	pH	−4.526	1.2122	−3.73	0.0039
	Adsorbent quantity	5.7177	1.2122	4.72	0.0008
	Adsorbat concentration	−5.204	1.2122	−4.29	0.0016
	pH*pH	−15.702	3.0647	−5.12	0.0004
MR	Constant	96.447	2.3898	40.359	<0.0001
	pH	−10.47	1.4171	−7.391	<0.0001
	Adsorbent quantity	13.106	1.4171	9.2482	<0.0001
	pH*Adsorbent quantity	7.5569	1.5307	4.937	0,0002
	Adsorbent quantity*Adsorbent quantity	−12.45	3.0373	−4.1	0.0011

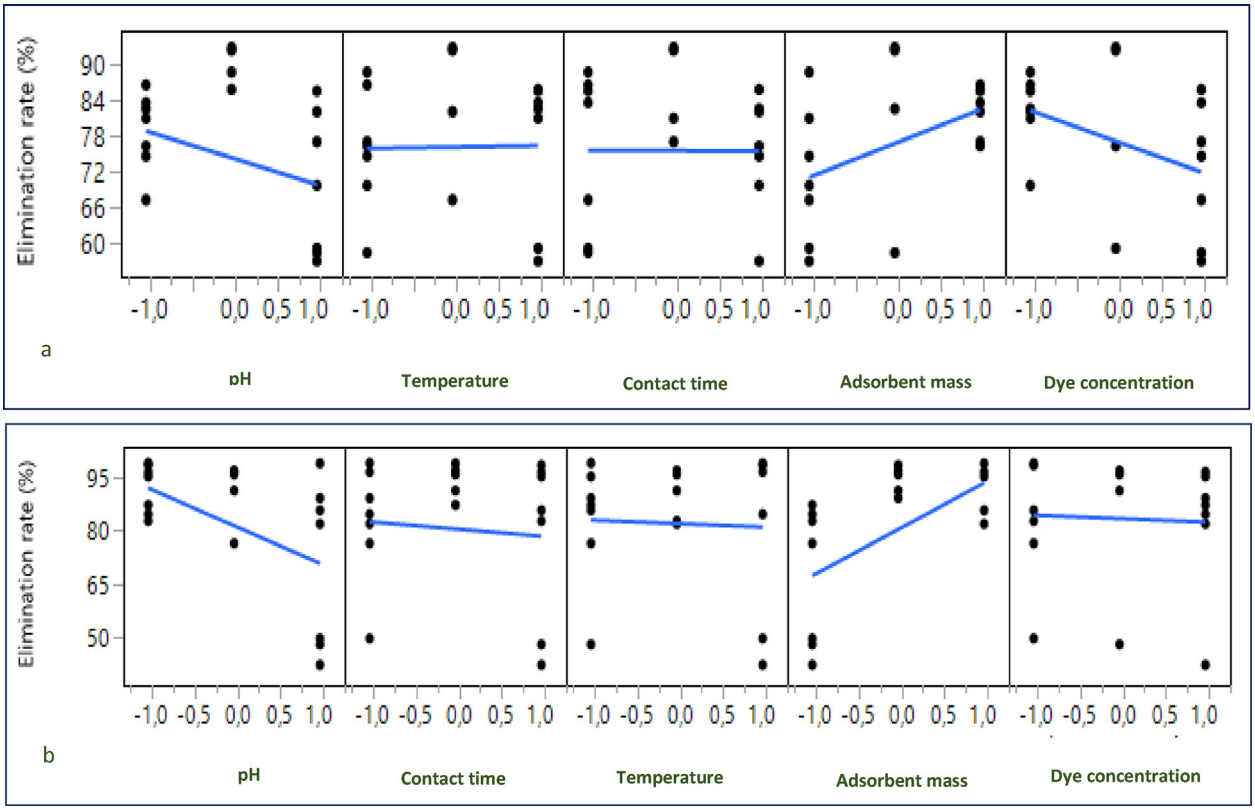

Fig. 2. Diagram of main effects on the removal rate of MG (a) and MR (b).

$$Ln(K_0) = \frac{-\Delta H^\circ}{R.T} + \frac{\Delta S^\circ}{R} \quad (10)$$

Where K_0 the apparent equilibrium constant, R the perfect gas constant and T the absolute temperature (K). The values of the equilibrium constant (K_0) for the adsorption were obtained according to the eq (11) [33]:

$$K_0 = \frac{C_e}{q_e} \quad (11)$$

3.1.5. Characterization of activated carbon after adsorption

The physicochemical properties of the activated carbon after adsorption were determined using a Jeol model it500 HR scanning electron microscope, a Panalytical X'Pert Pro X-ray diffractometer equipped with a Cu-Kα anode of monochromatic source (1.54 Å), set to an operating voltage of 40 KV and a filament current of 30 mA and a Bruker FT-IR Spectroscope model Vertex 70.

4. Results and discussion

4.1. Definitive screening design

The whole obtained data were fitted using JMP Pro software (SAS Institute Inc, 2018a) [20]. As mentioned previously, DSD provides a compelling balance between the number of variables to be modeled and the number of experiments to be performed, with an ability to detect main, interaction, and quadratic effects without the need for effect aliasing [34].

4.1.1. Evaluation of the DSD model

The accuracy of the multiple regression equations constructed by DSD was evaluated. The model selection was examined using the criteria of BIC "Bayesian information criterion", the Δ(BIC) must be greater than or equal to 2 [35,36], and then using statistical values including R^2_{ajd}, RMSE "*root mean squared error*" and p-value. Therefore, Table 3 gathers the ranking of the bars from largest to smallest according to a Pareto chart. A model with four terms was selected for the removal rate of both dyes. In the case of MG, this prediction model includes the main effects of adsorbent amount, dye concentration, pH, and the quadratic effect of pH. In the case of MR, it includes the main effects of adsorbent amount, pH, the quadratic effect of adsorbent amount, and the interaction of the two significant factors. The lack of fit test is not significant due to the p-value being greater than 0.05 for both dyes. The results of Table 4 indicate that any predictor left out of the model is considered insignificant and they show that the established model predicts well the experimental data.

The selected models provide a good description of the process since all individual observations (Y_{obs}) are in good agreement with the predicted values (Y_{pred}) and fall within the 95 % prediction intervals, as shown in the scatter plots of the experimental and

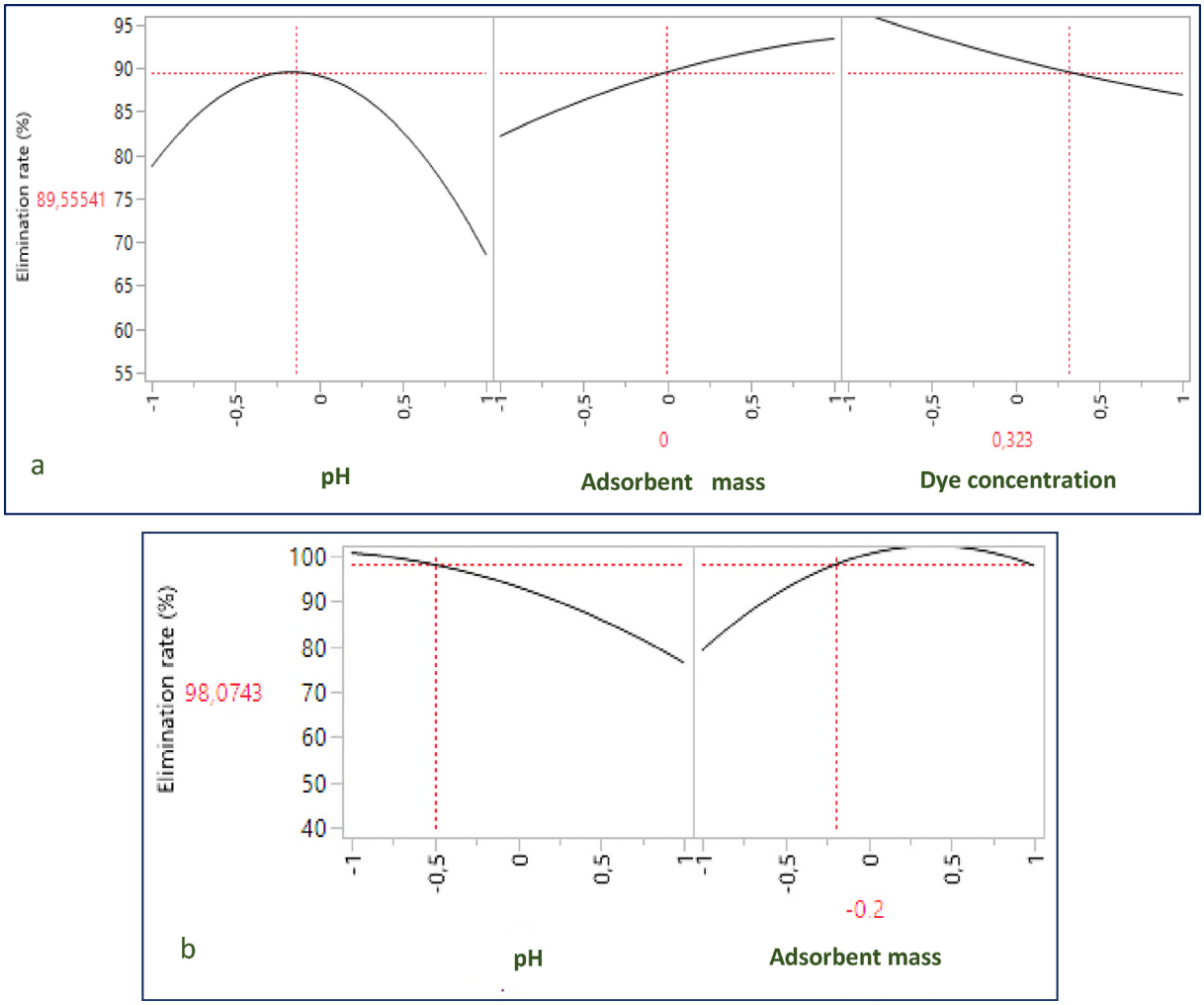

Fig. 3. Plot of optimal parameters for the adsorption of MG (a) and MR (b).

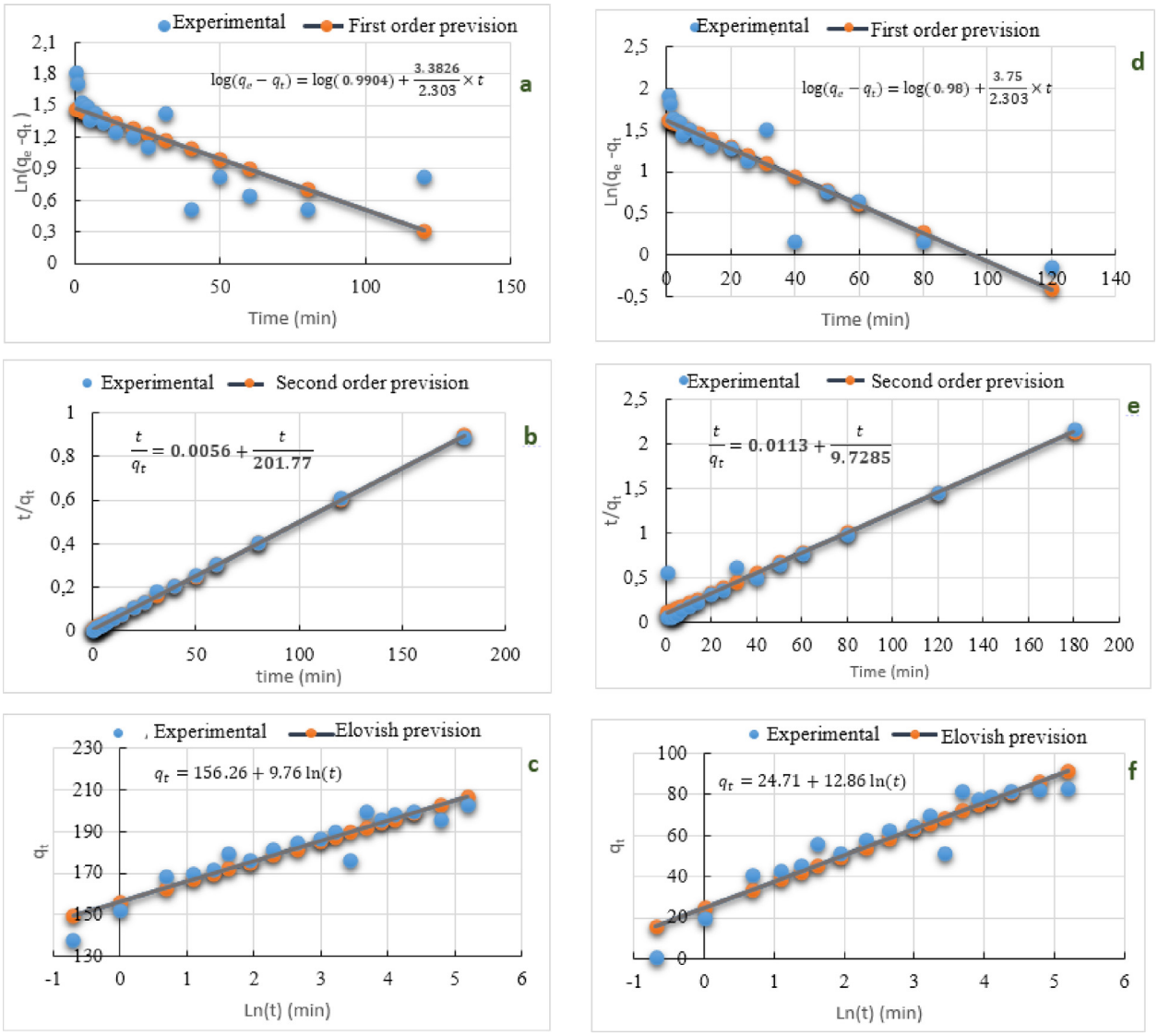

Fig. 4. Curves illustrating the kinetic model of adsorption on AC; pseudo-first order for MG (a) and for MR (d), pseudo-second order for MG (b) and for MR (e), Elovish for MG (c) and for MR (f), *DC = 100 ppm (MG), 50 ppm (MR), pH = 6 for (MG), pH = 2 for (MR), T = 25 °C.*

Table 6
Parameters and their validity criteria of the pseudo-first-order, pseudo-second-order, and Elovish model for the adsorption of dyes (MG and MR) on CA.

Kinetic model	Dye	Parameter	Value	Adjusted correlation coefficient	Standard deviation	*p-Value*
Pseudo-first order	MG	q_e (mg.g^{-1})	0.9905	0.6203	0.2582	0.0002
		k_f (min^{-1})	−3.3826			
	MR	q_e (mg.g^{-1})	0.9832	0.8323	0.2621	0.0000
		k_f (min^{-1})	−3.7465			
Pseudo-second order	MG	q_e (mg.g^{-1})	201.7671	0.9994	0.0061	0.0000
		k_f (min^{-1})	0.0044			
	MR	q_e (mg.g^{-1})	88.4052	0.9505	0.1285	0.0000
		k_f (min^{-1})	0.0012			
Elovish	MG	α (mg.g^{-1}.min^{-1})	−7.0264	0.8853	6.0568	0.0000
		β (g.min^{-1})	0.1024			
	MR	α (mg.g^{-1}.min^{-1})	−0.7519	0.8888	7.8452	0.0000
		β (g.min^{-1})	0.0777			

predicted values (Fig. 1). The calculated coefficients of determination adjusted by the degrees of freedom (R^2_{ajd}) are very high. These values are 0.94 and 0.92 for MG and MR respectively with p-values less than 0.05. The significant factors evaluated explain well the removal rates of both dyes.

The probability values represented in Table 5 indicate that the statistically significant model factors for MG are the amount of adsorbent, pH, the quadratic effect of the amount of adsorbent, and the interaction of the two factors. While for the MR case, the

main effects are the amount of adsorbent, dye concentration, pH, and the quadratic effect of pH.

4.1.2. Screening effects

The mode of the contribution of each factor on the removal rate for both dyes is collected in Table 5 and described in Fig. 2. The pH shows a remarkable negative effect on the removal rate of both dyes ($p < 0.001$) (Fig. 2), this is due to the acidic nature of the used activated carbon ($pH_{pzc} = 4.5$) (Table 1). The significant increase in the amount of adsorbent has a positive effect on the response ($p < 0.001$) (Table 5) the number of adsorption sites is proportional to the dispersed amount of adsorbent, thus favoring the retention of both dyes. The same observation was noted by Larous et al. [36]. The concentration of the dye shows a negative effect on the retention of the MG of cationic nature. This is justified by the establishment of a plateau indicating an equilibrium state resulting from the saturation of the active sites. [37] (Fig. 2, b). Temperature and duration do not have significant effects and therefore do not greatly influence the desired response, i.e., the process is not affected by temperature variation. Other studies [36] have shown that a contact time of 5 to 10 min is more than sufficient to have maximum dye retention.

The models that can be used to predict the results are illustrated by equations (12) for MG and (13) for MR:

$$ER = 96.45 - 10.47.pH + 13.01.Adsorbentquantity + 7.56.pH.Adsorbentquantity - 12.45.(Adsorbantquantity)^2 \quad (12)$$

$$ER = 90.95 - 4.53.pH + 5.71.Adsorbent\ quantity + 7.56.Adsorbat\ concentration - 15.70.(pH)^2 \quad (13)$$

4.1.3. Optimization

The plot of optimal process parameters to maximize removal rates shows that the optimal pH is 6 for MG and 3 for MR, the amount of adsorbent is 0.05 g for both dyes, and an optimal MG concentration of 100 ppm (Fig. 3). The predicted values of maximum removal rates are 96.037 % for MG and 98.07 % for MR. Confirmatory experiments yield maximum removal rates of 93.81 % for MG and 82.81 % for MR, which is in good agreement with the predicted value from the model equations (12) and (13).

4.2. Kinetics of adsorption

In order to model the adsorption kinetics of MG and MR on AC, three models were used. The modeling curves are collected in Fig. 4. From the linearity study of the experimental data and those predicted from the models, it is concluded that the adsorption process follows the pseudo-second-order model for both dyes.

The kinetic constants, fitted coefficient of determination, standard deviation, and probability value show better agreement with the pseudo-second-order kinetic model for both dyes. Indeed, the fitted correlation coefficient (R^2_{ajd}) is greater than 0.99 for MG and greater than 0.95 for MR, with the lowest standard deviation (Table 6) and agreement between the experimental and calculated maximum adsorption capacities [37]. The pseudo-second-order kinetic model well describes the adsorption phenomenon through the establishment of chemical bonds (interactions) between the adsorbates and the functional groups on the surface of the adsorbents that are responsible for the adsorption capacity of the adsorbents [38,39]. The equations of the pseudo-second-order model are Eq. (14) and Eq. (15) for the MG and the MR respectively. These results are in good agreement with the studies of El Hajam et al [40] and Hassan et al [41].

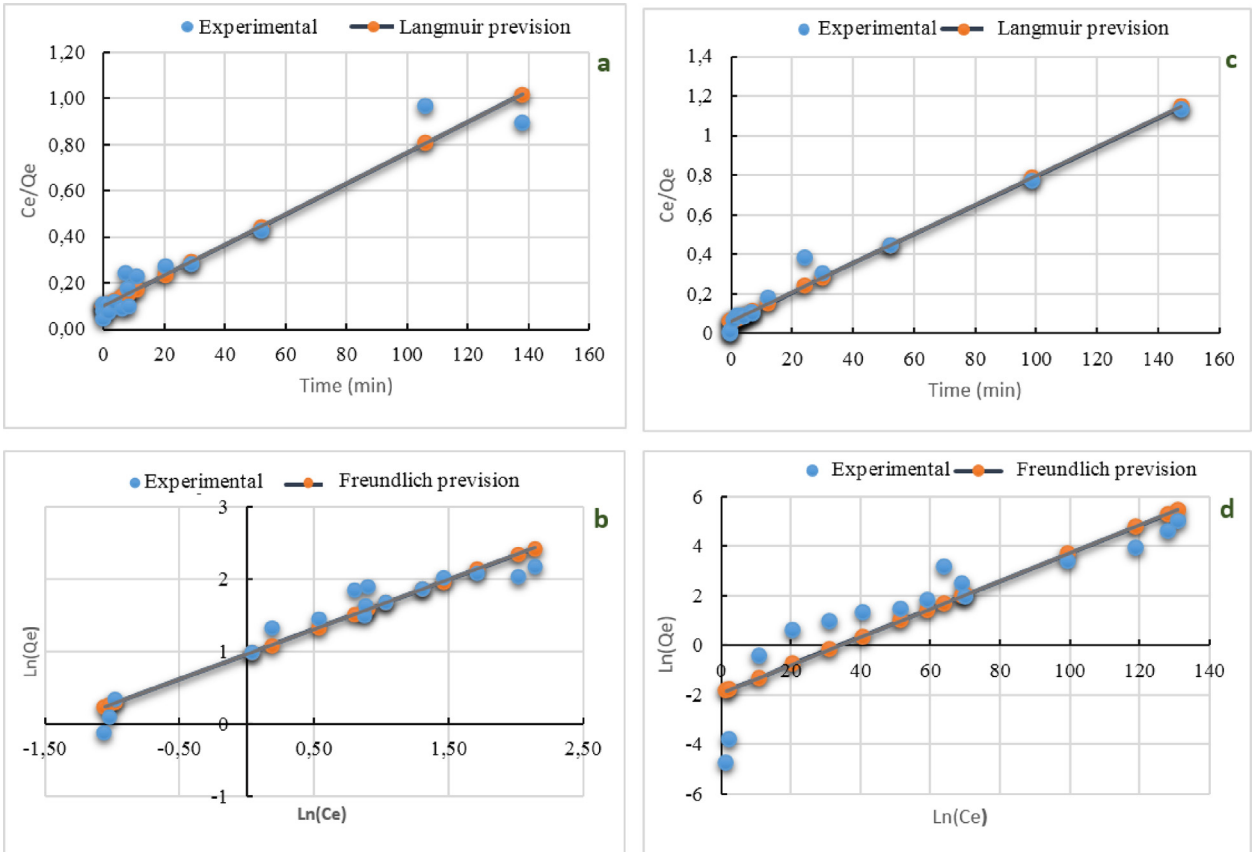

Fig. 5. Modeling of adsorption isotherms of the two dyes on AC; Langmuir for MG (a) and MR (c) and Freundlich for MG (b) and MR (d).

Table 7
Parameters of the different isothermal models for the study of the adsorption of MG and MR dyes on CA at 298 °K.

Isothermal models	dye	parameter	value	Adjusted correlation coefficient	Standard deviation	*p-Value*
Langmuir	MG	q_m (mg.g^{-1})	150.68	0.9396	0.0685	3.892×10^{-10}
		k_l (l.mg^{-1})	0.07			
	MR	q_m (mg.g^{-1})	135.89	0.9785	0.0474	4.491×10^{-13}
		k_f (l.mg^{-1})	0.12			
Freundlich	MG	1/n	0.68	0.9229	0.2090	$3{,}526 \times 10^{-09}$
		k_f	9.25			
	MR	1/n	0.06	0.7968	1.2961	7.596×10^{-06}
		k_f	0.01			

$$\frac{t}{q_t} = 0.0056 + \frac{t}{201.77} \quad (14)$$

$$\frac{t}{q_t} = 0.0113 + \frac{t}{9.7285} \quad (15)$$

4.3. Adsorption isotherms

Analysis of the linear fitted Langmuir and Freundlich adsorption isotherm curves for both dyes from the experimental data at 298 °K reveals that the Langmuir adsorption model sufficiently fits the data (Fig. 5). This is confirmed by the parameters of the regression method namely the fitted correlation coefficients (R^2_{ajd}), the low values of the standard deviation between the experimental and calculated values (Table 7). The Langmuir constant q_m is significant, justifying the maximum adsorption capacity at equilibrium [42]. The difference in the values of the K_L constants denoting the adsorption energy and affinity of the binding sites of MG and MR can be explained by the difference in the binding strength of the dyes and the surface area of the AC [3,43]. The Freundlich model cannot explain the equilibrium adsorption phenomenon, due to its low R^2_{ajd} (0.93). Similar findings were reported on the adsorption of MG onto activated carbon prepared from the epicarp of Ricinus communis [44] and Coconut Shell activated carbon [45], and the adsorption of MR on Annona squamosal shell [46].

4.4. Thermodynamic study

The thermodynamic study of the adsorption of the two dyes on the AC allows us to calculate the different thermodynamic functions, the negative obtained values of ΔH°, indicate the exothermic nature of this adsorption (Table 8). The positive values of ΔS° show that the adsorption is a spontaneous process, however, it should also be noted that the entropy of adsorption and the external medium may increase due to the exothermic nature of the phenomenon [47], as the system is open. The decrease in ΔG° values with increasing temperature shows that adsorption becomes less favorable at higher temperatures [48]. This is because the increase in temperature promotes the mobility of the dye molecules and causes the desorption of its molecules from the solid phase. Therefore, the adsorption capacity decreases with increasing solution temperature, moreover, the values of equilibrium constants K_0 (Table 3) show that the mobility of the dye molecules increases with increasing temperature, revealing a low affinity of CA towards both dyes at high temperatures [49].

4.5. Characterization of activated carbon after adsorption

SEM observation of the AC surfaces after adsorption shows saturation of the pores by dye particles. The appearance of a molecular cloud on the dye-loaded adsorbent surface indicates good adhesion of the dye ions to the functional groups present in the AC (Fig. 6 a, b).

The analysis of the infrared absorption spectrum of CA after adsorption of the MG dye indicates the presence of the functional groups characteristic of the latter (Fig. 6, c). Thus, we note an intense band at 3400 cm^{-1} attributed to the vibration of the primary amine group (NH_3). The band at 2990 cm^{-1} corresponds to the vibration of the bond C = CH characteristic of the benzylic rings [50], and the band of adsorption at 1700 cm^{-1} corresponds to the elongation of the bonds C=N [51]. On the other hand, one observes a band at 1230 cm^{-1} corresponds to the elongation of the bond

Table 8
Calculated thermodynamic functions ΔG°, ΔS°, and ΔH° of MG and MR upon adsorption on AC.

Dye	T (°K)	K_0	ΔG° (kJ. mol^{-1})	ΔH° (J. mol^{-1})	ΔS° (J.K^{-1}. mol^{-1})
MG	288	0.7026	0.8453	−7.1259	20.3959
	293	0.6442	1.0711		
	298	0.5192	1.6241		
	303	0.6768	0.9835		
	308	0.7204	0.8396		
	313	0.7389	0.7874		
	323	0.8412	0.4642		
	333	0.8875	0.3304		
	343	0.9504	0.1450		
	353	1.0650	−0.1848		
MR	288	0.4628	1.8446	−6.9849	16.2143
	293	0.4272	2.0720		
	298	0.3477	2.6174		
	303	0.3989	2.3154		
	308	0.4523	2.0315		
	313	0.4846	1.8850		
	323	0.5443	1.6336		
	333	0.5704	1.5541		
	343	0.6053	1.4318		
	353	0.6665	1.1907		

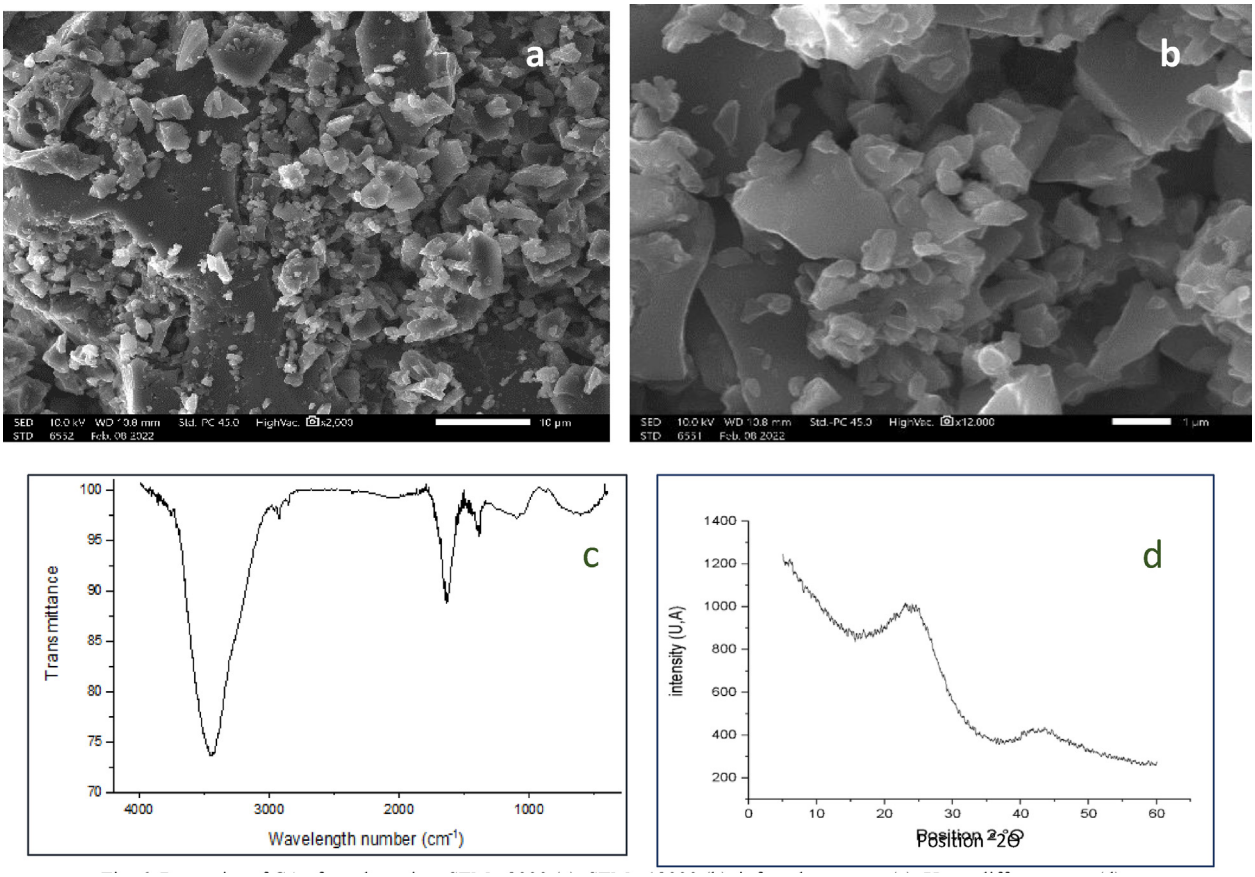

Fig. 6. Properties of CA after adsorption, SEM × 2000 (a), SEM × 12000 (b), infrared spectrum (c), X-ray diffractogram (d).

C—O, another band around 1440 cm^{-1} is allotted to the vibration of the valence of the groups, O—H, and the band around 885 cm^{-1} allotted to the vibration of bond C=C characteristic of the used CA [52].

The X-ray diffractogram of Activated Carbon after adsorption is shown in Fig. 6.d, it shows two broad peaks characteristic of CA, showing that the structure of the adsorbent material remains intact without any change in its graphite structure of the carbon which is essentially amorphous predominant [53].

5. Adsorption comparative study

The maximum adsorption capacity (Q_m) values, computed from the Langmuir model, of AC particles and various adsorbents studied in the literature are summarized in Table 9. This study showed that the maximum adsorption capacity of AC particles is 150.68 and 135.89 mg/g for MG and MR, respectively. It can be seen that the AC particles exhibit superior MG and MR uptake capacity to that of previously reported adsorbents. Thus, these results show that Almond shell activated carbon, which is a readily available and cheap by-product, can be utilized as a potential adsorbent to reduce the concentration of cationic and anionic dyes from contaminated water.

Table 9
Maximum adsorption capacities of MG and MR on various adsorbents.

Adsorbent	Dye	Qm (mg/g)	Reference
Almond shell activated carbon	MG	150.68	Present study
Coconut Shell activated carbon	MG	78.11	[45]
Activated Epicarp of Ricinus communis	MG	20.4081	[44]
almond shell bioadsorbent	MG	126.90	[54]
Almond shell activated carbon	MR	135.89	Present study
Lemongrass leaf activated carbon	MR	76.923	[55]
Annona squmosa activated carbon	MR	40.486	[37]
Activated Carbon	MR	7.26	[56]

6. Conclusion

Activated carbon based on Almond shells used as adsorbent for two types of dyes namely Malachite Green and Methyl Red allows removal up to 93.81 % and 82.81 % respectively. Screening and optimization of five variables influencing the adsorption process are performed using a new design of experiments methodology called the definitive screening design (DSD) to maximize the removal rate (%R). Mathematical models are developed to predict this response for each dye and show a good correlation between the predicted and experimental results. According to the optimization step, the optimal pH values are 6 for MG and 3 for MR, the amount of adsorbent is 0.05 g for both dyes and an optimal concentration of 100 ppm in the case of MG. The other factors do not have a significant effect on the desired response.

The kinetic study shows that the adsorption is of pseudo-second order type for both dyes with a boundary layer of 56.4 mg/g. The equilibrium isotherms reveal that the adsorption of the two dyes on activated carbon is well adapted to the Langmuir model with a maximum capacity of 150.68 for MG and 135.89 mg/g for MR, which reveals a great affinity of adsorption towards the dyes of cationic nature. The thermodynamic study shows the spontaneous and exothermic nature of the adsorption process for both dyes, this

is justified by the negative enthalpy (ΔH°) and positive entropy (ΔS°) values. Characterization of the activated carbon after the adsorption process shows an interesting adsorption efficiency towards the particles of both dyes.

CRediT authorship contribution statement

H. Boulika: Conceptualization, Visualization, Data curation, Investigation, Methodology, Writing – original draft. **M. El Hajam:** Visualization, Writing – review & editing. **M. Hajji Nabih:** Data curation, Investigation. **I. Riffi Karim:** Data curation, Investigation. **N. IDRISSI KANDRI:** Conceptualization, Formal analysis, Methodology. **A. Zerouale:** Writing – review & editing, Validation.

Data availability

No data was used for the research described in the article.

Declaration of Competing Interest

The authors declare that they have no known competing financial interests or personal relationships that could have appeared to influence the work reported in this paper.

Reference

[1] W. Konicki, D. Sibera, E. Mijowska, Z. Lendzion-Bieluń, U. Narkiewicz, Equilibrium and kinetic studies on acid dye Acid Red 88 adsorption by magnetic ZnFe2O4 spinel ferrite nanoparticles, J. Colloid Interface Sci. 398 (2013) 152–160, https://doi.org/10.1016/j.jcis.2013.02.021.
[2] M. El Hajam, N. Idrissi Kandri, A. Harrach, A. El khomsi, A. Zerouale, Adsorption of Methylene Blue on industrial softwood waste 'Cedar' and hardwood waste 'Mahogany': Comparative study, Mater. Today Proc. 13 (2019) 812–821.
[3] M.A. El-bindary, M.G. El-desouky, A.A. El-bindary, Adsorption of industrial dye from aqueous solutions onto thermally treated green adsorbent: A complete batch system evaluation, J. Mol. Struct. 346 (2022), https://doi.org/10.1016/j.molliq.2021.117082.
[4] A. Mittal, Adsorption kinetics of removal of a toxic dye, Malachite Green, from wastewater by using hen feathers, J. *Hazard. Mater.* 133 (2006) 196–202, https://doi.org/10.1016/j.jhazmat.2005.10.017.
[5] C. Sahoo, A.K. Gupta, A. Pal, Photocatalytic degradation of Methyl Red dye in aqueous solutions under UV irradiation using Ag + doped TiO 2, Desalination 181 (2005) 91–100, https://doi.org/10.1016/j.desal.2005.02.014.
[6] X. Zhu, L.i. Qiao, P. Ye, B. Ying, J. Xu, C. Shen, P. Zhang, Copper-catalyzed rapid C–H nitration of 8-aminoquinolines by using sodium nitrite as the nitro source under mild conditions, RSC Adv. 6 (92) (2016) 89979–89983.
[7] I. Kiran, T. Akar, A.S. Ozcan, A. Ozcan, S. Tunali, Biosorption kinetics and isotherm studies of Acid Red 57 by dried Cephalosporium aphidicola cells from aqueous solutions, Biochem. Eng. J. 31 (3) (2006) 197–203.
[8] X. He, M. Du, H. Li, T. Zhou, Removal of direct dyes from aqueous solution by oxidized starch cross-linked chitosan/silica hybrid membrane, Int. J. Biol. Macromol. 82 (2016) 174–181, https://doi.org/10.1016/j.ijbiomac.2015.11.005.
[9] M. Neamtu, A. Yediler, I. Siminiceanu, M. Macoveanu, A. Kettrup, Decolorization of disperse red 354 azo dye in water by several oxidation processes—a comparative study, Dyes and Pigments 60 (1) (2004) 61–68.
[10] Y.S. Shankar, K. Ankur, P. Bhushan, Utilization of Water Treatment Plant (WTP) Sludge for Pretreatment of Dye Wastewater Using Coagulation/ Flocculation. *Advances*, Waste Management. (2019) 107–121, https://doi.org/10.1007/978-981-13-0215-2.
[11] K.C. Chen, J.Y. Wu, C.C. Huang, Y.M. Liang, S.C.J. Hwang, Decolorization of azo dye using PVA-immobilized microorganisms, J. Biotechnol. 101 (2003) 241–252, https://doi.org/10.1016/S0168-1656(02)00362-0.
[12] R. Gong, Y. Ding, M. Li, C. Yang, H. Liu, Y. Sun, Utilization of powdered peanut hull as biosorbent for removal of anionic dyes from aqueous solution, Dye. Pigment. 64 (2005) 187–192, https://doi.org/10.1016/j.dyepig.2004.05.005.
[13] H. Ait Ahsaine, M. Zbair, Z. Anfar, Y. Naciri, R. El haouti, N. El Alem, M. Ezahri, Cationic dyes adsorption onto high surface area 'almond shell' activated carbon: Kinetics, equilibrium isotherms and surface statistical modeling, Mater. Today Chem. 8 (2018) 121–132.
[14] G.A.A. Alhazmi, K.S. Aboumelha, M.G. El-desouky, A.A. El-bindary, Effective adsorption of doxorubicin hydrochloride on zirconium metal-organic framework : Equilibrium, kinetic and thermodynamic studies, j mol struct. 1258 (2022) 1–15, https://doi.org/10.1016/j.molstruc.2022.132679.
[15] J. Acharya, J.N. Sahu, B.K. Sahoo, C.R. Mohanty, B.C. Meikap, Removal of chromium(VI) from wastewater by activated carbon developed from Tamarind wood activated with zinc chloride, Chem. Eng. J. 150 (2009) 25–39, https://doi.org/10.1016/j.cej.2008.11.035.
[16] E. Demirbas, M. Kobya, A.E.S. Konukman, Error analysis of equilibrium studies for the almond shell activated carbon adsorption of Cr(VI) from aqueous solutions, J. Hazard. Mater. 154 (2008) 787–794, https://doi.org/10.1016/j.jhazmat.2007.10.094.
[17] D. Mohan, A. Sarswat, V.K. Singh, M. Alexandre-Franco, C.U. Pittman, Development of magnetic activated carbon from almond shells for trinitrophenol removal from water, Chem. Eng. J. 172 (2-3) (2011) 1111–1125.
[18] S. Hashemian, K. Salari, Z.A. Yazdi, Preparation of activated carbon from agricultural wastes (almond shell and orange peel) for adsorption of 2-pic from aqueous solution, J. Ind. Eng. Chem. 20 (2014) 1892–1900, https://doi.org/10.1016/j.jiec.2013.09.009.
[19] B. Jones, C.J. Nachtsheim, A class of three-level designs for definitive screening in the presence of second-order effects, J. Qual. Technol. 43 (2011) 1–15, https://doi.org/10.1080/00224065.2011.11917841.
[20] A. Erler, N. Mas, P. Ramsey, G. Henderson, Efficient biological process characterization by definitive-screening designs: The formaldehyde treatment of a therapeutic protein as a case study, Biotechnol. Lett. 35 (2013) 323–329, https://doi.org/10.1007/s10529-012-1089-y.
[21] G. Peter, B. Jones, Optimal design of experiments a case study approach, John Wiley, Hoboken, N.J, 2011, 10.1002/9781119974017.
[22] N.K. Nguyen, S. Stylianou, Constructing definitive screening designs using cyclic generators, J. Stat. Theory Pract. 7 (2013) 713–724, https://doi.org/10.1080/15598608.2013.781891.
[23] W. Libbrecht, F. Deruyck, H. Poelman, A.n. Verberckmoes, J. Thybaut, J. De Clercq, P. Van Der Voort, Optimization of soft templated mesoporous carbon synthesis using Definitive Screening Design, Chem. Eng. J. 259 (2015) 126–134.
[24] G.E.P. Box, D.R. Cox, An Analysis of Transformations, J R Stat Soc Ser B. 26 (1964) 211–243, https://doi.org/10.1111/j.2517-6161.1964.tb00553.x.
[25] S. Lagergren, About the Theory of So-called Adsorption of Soluble Substances, Handingarl. 24 (1898) 1–39.
[26] Y.S. Ho, G. McKay, Pseudo-second order model for sorption processes, Process Biochem. 34 (5) (1999) 451–465.
[27] M.J.D. Low, Kinetics of chemisorption of gases on solids, Chem. Rev. 60 (1960) 267–312, https://doi.org/10.1021/cr60205a003.
[28] M. El Hajam, N.I. Kandri, G.-I. Plavan, A.H. Harrath, L. Mansour, F. Boufahja, A. Zerouale, Pb^{2+} ions adsorption onto raw and chemically activated Dibetou sawdust: Application of experimental designs, J. King Saud Univ. - Sci. 32 (3) (2020) 2176–2189.
[29] V.K. Gupta, T.A. Saleh, Sorption of pollutants by porous carbon, carbon nanotubes and fullerene- An overview, Environ. Sci. Pollut. Res. 20 (2013) 2828–2843, https://doi.org/10.1007/s11356-013-1524-1.
[30] M.H. Armbruster, J.B. Austin, The Adsorption of Gases on Plane Surfaces of Mica, J. Am. Chem. Soc. 60 (2) (1938) 467–475.
[31] H. Freundlich, H. Wilpried, The Adsorption of cis- and trans-Azobenzene, J. Am. Chem. Soc. 61 (1939) 2228–2230, https://doi.org/10.1021/ja01877a071.
[32] Q. Li, Q.Y. Yue, Y. Su, B.Y. Gao, H.J. Sun, Equilibrium, thermodynamics and process design to minimize adsorbent amount for the adsorption of acid dyes onto cationic polymer-loaded bentonite, Chem. Eng. J. 158 (2010) 489–497, https://doi.org/10.1016/j.cej.2010.01.033.
[33] E.J. Ward, A review and comparison of four commonly used Bayesian and maximum likelihood model selection tools, Ecol. Modell. 211 (2008) 1–10, https://doi.org/10.1016/j.ecolmodel.2007.10.030.
[34] K.P. Burnham, D.R. Anderson, Multimodel inference: Understanding AIC and BIC in model selection, Sociol. Methods Res. 33 (2) (2004) 261–304, https://doi.org/10.1177/0049124104268644.
[35] K. Takagaki, T. Ito, H. Arai, Y. Obata, K. Takayama, Y. Onuki, The usefulness of definitive screening design for a quality by design approach as demonstrated by a pharmaceutical study of orally disintegrating tablet, Chem Pharm Bull. 67 (2019) 1144–1151, https://doi.org/10.1248/cpb.c19-00553.
[36] S. Larous, A.H. Meniai, Adsorption of Diclofenac from aqueous solution using activated carbon prepared from olive stones, Int. J. Hydrogen Energy 41 (2016) 10380–10390, https://doi.org/10.1016/j.ijhydene.2016.01.096.
[37] T. Santhi, S. Manonmani, T. Smitha, Removal of methyl red from aqueous solution by activated carbon prepared from the *Annona squmosa* seed by adsorption, Chem. Eng. Res. Bull. 14 (2010) 11–18, https://doi.org/10.3329/cerb.v14i1.3767.
[38] Z. Hussain, R. Kumar, D. Meghavathu, Kinetics and thermodynamics of adsorption process using a spent-FCC catalyst, Int. J. Eng. Technol. 7 (2018) 284–287, https://doi.org/10.14419/ijet.v7i4.5.20090.
[39] A.M. Aljeboree, A.N. Alshirifi, A.F. Alkaim, Kinetics and equilibrium study for the adsorption of textile dyes on coconut shell activated carbon, Arab. J. Chem 10 (2017) S3381–S3393, https://doi.org/10.1016/j.arabjc.2014.01.020.
[40] M. El Hajam, N.I. Kandri, A. Harrach, A. Zerouale, Adsorptive removal of brilliant green dye from aqueous solutions using cedar and mahogany sawdusts, Sci Study Res Chem Eng Biotechnol Food Ind. 20 (2019) 395–409.
[41] N. Hassan, A. Shahat, A. El-didamony, M.G. El-desouky, A.A. El-bindary, Mesoporous iron oxide nano spheres for capturing organic dyes from water sources, J. Mol. Struct. 1217 (2020) 1–15, https://doi.org/10.1016/j.molstruc.2020.128361.
[42] T.A. Altalhi, M.M. Ibrahim, G.A.M. Mersal, et al., Adsorption of doxorubicin hydrochloride onto thermally treated green adsorbent: Equilibrium, kinetic and thermodynamic studies, J. Mol. Struct. 1263 (2022) 1–11, https://doi.org/10.1016/j.molstruc.2022.133160.
[43] A. Ergene, K. Ada, S. Tan, H. Katircioğlu, Removal of Remazol Brilliant Blue R dye from aqueous solutions by adsorption onto immobilized Scenedesmus

quadricauda: Equilibrium and kinetic modeling studies, Desalination. 249 (2009) 1308–1314, https://doi.org/10.1016/j.desal.2009.06.027.
[44] M. Makeswari, T. Santhi, Removal of Malachite Green Dye from Aqueous Solutions onto Microwave Assisted Zinc Chloride Chemical Activated Epicarp of Ricinus communis, Water Resour Prot. 5 (2013) 222–238.
[45] S.A.H. Azaman, A. Afandi, B.H. Hameed, A.T.M. Din, Removal of Malachite Green from Aqueous Phase Using Coconut Shell Activated Carbon : Adsorption, Desorption, and Reusability Studies, JASE. 21 (3) (2018) 317–330, https://doi.org/10.6180/jase.201809.
[46] E.A. Khan, Shahjahan, T.A. Khan, Adsorption of methyl red on activated carbon derived from custard apple (Annona squamosa) fruit shell: Equilibrium isotherm and kinetic studies, J Mol Liq. 249 (2018) 1195–1211.
[47] H.M. El, N.I. Kandri, A. Zerouale, Batch adsorption of Brilliant Green dye on raw Beech sawdust : Equilibrium isotherms and kinetic studies. 3 (2019) 431–435.
[48] S. Chowdhury, R. Mishra, P. Saha, P. Kushwaha, Adsorption thermodynamics, kinetics and isosteric heat of adsorption of malachite green onto chemically modified rice husk, Desalination 265 (2011) 159–168, https://doi.org/10.1016/j.desal.2010.07.047.
[49] N. Hassan, A. Shahat, A. El-didamony, M.G. El-desouky, A.A. El-bindary, Synthesis and characterization of ZnO nanoparticles via zeolitic imidazolate framework-8 and its application for removal of dyes, j mol struct. 1210 (128029) (2020) 1–15, https://doi.org/10.1016/j.molstruc.2020.128029.
[50] G. Socrates, Infrared and Raman Characteristic Group Frequencies Tables and Charts, John Wiley & Sons, New York, 1980, 10.1016/0003-2670(94)80274-2.
[51] M. Hajji Nabih, M. El Hajam, H. Boulika, M.M. Hassan, N. Idrissi Kandri, A. Hedfi, A. Zerouale, F. Boufahja, Physicochemical Characterization of Cardoon ' Cynara cardunculus ' Wastes (Leaves and Stems), A Comparative Study 13 (24) (2021) 13905.
[52] A.S. Politou, C. Morterra, M.J.D. Low, Infrared studies of carbons. XII The formation of chars from a polycarbonate, Carbon N. Y. 28 (4) (1990) 529–538.
[53] J. Zhao, L. Yang, F. Li, R. Yu, C. Jin, Structural evolution in the graphitization process of activated carbon by high-pressure sintering, Carbon N. Y. 47 (2009) 744–751, https://doi.org/10.1016/j.carbon.2008.11.006.
[54] R. Ben, A. Sarra, K. Karine, M. Achraf, Adsorptive removal of cationic and anionic dyes from aqueous solution by utilizing almond shell as bioadsorbent, Euro-Mediterr J Env Integr. 2 (2017) 1–13, https://doi.org/10.1007/s41207-017-0032-y.
[55] M. Azmier, N. Adilah, B. Ahmed, K. Adesina, O. Solomon, Sorption studies of methyl red dye removal using lemon grass (Cymbopogon citratus), CDC. 22 (2019) 1–11, https://doi.org/10.1016/j.cdc.2019.100249.
[56] A. Usman, V.C. Ugboaja, Pseudo Constants for Methyl Red Sorption: A Rate Study of Received and Derived Activated Carbon, JEAS 1 (2011) 1–9, https://doi.org/10.4236/jeas.2011.14008.